



Sustainable Energy Fuels, 2018, 2, 229

A

IC₂ff

†

Tingting Tang,^{†a} Qiuping Gan,^{†a} Xiaohui Guo,^a Hailin Dong,^{*b} Jifang Zhang,^a Yanchun Zhao,^{*a} Jianniao Tian^{ID}^a and Xiulin Yang^{ID}^{*a}

Herein, a hybrid catalyst of Pt/CoNiO₂ on carbon nanotubes (Pt/CoNiO₂-CNTs) has been successfully synthesized by a facile and cost-effective method, and its crystal structures, chemical valence states, and morphologies have been characterized in detail. CO stripping voltammograms reveal that the adsorbed CO_{ads} on the active sites of the Pt/CoNiO₂-CNT catalyst is easily oxidized at a lower potential (−0.60 V) as compared to the Pt particles on rGO (−0.35 V) and acid-treated CNTs (−0.36 V). Cyclic voltammograms demonstrate that the designed Pt/CoNiO₂-CNT catalyst possesses an ultrahigh electrocatalytic activity (1136.2 mA mg_{Pt}^{−1}) for ethanol oxidation, which is 5.1 and 3.0 times higher than that of Pt/rGO (221.6 mA mg_{Pt}^{−1}) and Pt/CNTs (375.4 mA mg_{Pt}^{−1}), respectively. The Tafel plot of Pt/CoNiO₂-CNTs is 205 mV dec^{−1}, indicating much faster reaction kinetics than that of the compared catalysts. In addition, the outstanding long-term stability indicates that the designed Pt/CoNiO₂-CNT catalyst exhibits expected application prospects in direct alkaline ethanol fuel cells. Moreover, the catalytic mechanism of the hybrid Pt/CoNiO₂-CNTs has been proposed and discussed *via* C2 and C1 pathways with respect to the final products for CH₃COO[−] and CO₃^{2−}, respectively.

Received 10th August 2017
Accepted 24th October 2017

DOI: 10.1039/c7se00392g

View Article Online

DOI: 10.1039/c7se00392g

With the increasing global warming and pollution, more countries and organizations are paying more attention to sustainable energy development.^{1,2} Low-carbon innovation and renewable energy technologies, such as fuel cells, solar cells *etc.*,³ have already spread in every step of the past few decades; among these, efficient fuel cell devices can directly convert chemical energy into electricity with almost no pollution except for some CO₂ gas.^{4,5} Especially, direct alcohol fuel cells have attracted significant attention due to their unique advantages such as flexible raw materials, being lightweight, and easy operations.^{6,7} Because of their much quicker fuel oxidation and oxygen reduction kinetics, direct alkaline fuel cells (DAFC) have been developed as one of the most sophisticated fuel cells as compared to the acid fuel cells as long-term power sources.^{8–12}

Moreover, the ease of poisoning nature of P-based catalysts in an acidic solution is another driving force that promotes the development of alkaline fuel cells.^{13–16}

Recently, oxygen reduction reactions in an alkaline solution have been rapidly developed, and outstanding progress has been made in the aspects of mechanistic study and catalytic performance.^{17–19} However, most of the designed alkaline anode catalysts, including P-based anode catalysts, are kinetically sluggish and do not satisfy the requirements for practical applications.^{20–23} Spendel and Wiecko's discovery of P-based catalysts in alkaline media over the past few decades and the introduction of noble metal loading, particle size distribution, and CO poisoning of P are the most important barriers inhibiting the development of these catalysts.²⁴ Therefore, it is urgent to develop effective strategies to improve the activity and durability of P-based catalysts in alkaline alcohol fuel cells.

Previous studies have revealed that transition metal oxides can resist alkaline corrosion and help to improve their ability of an i-CO poisoning in fuel cells.^{25–27} Among them, spinel nickel cobaltite (CoNiO₂), which has a relatively low price and exhibits an ironmenall friendly feature, has attracted significant attention.^{28,29} Some studies have shown that the earth-abundant CoNiO₂ possesses excellent electrochemical properties and exhibits a much higher electrical conductivity than cobalt

^aKey Laboratory for the Chemistry and Molecular Engineering of Medicinal Resources, Ministry of Education of China, College of Chemistry and Pharmacy, Guangxi Normal University, Guilin 541004, P. R. China. E-mail: xiulin.yang@kaust.edu.sa; yanchunzhao@aliyun.com

^bCatalysis and Chiral Technologies (CCT), Johnson Matthey (Shanghai) Catalyst Co., Ltd., Shanghai 201613, P. R. China. E-mail: donghl1980@126.com

† Electronic supplementary information (ESI) available. See DOI: 10.1039/c7se00392g

‡ These authors contributed equally.

oxides or nickel oxides alone.³⁰ In addition, CoNiO₂, as a high active catalyst, has been extensively explored in the water splitting reaction in alkaline media over the past few years.^{31–33} However, applications of CoNiO₂ in direct alkaline ethanol fuel cells are quite rare; thus, the study of CoNiO₂-based hybrid materials as an efficient anode catalyst is still highly significant.

In this study, we have successfully synthesized the P/CoNiO₂-CNT hybrid material, in which the P particles are uniformly dispersed on the surface of a CoNiO₂-CNT support by a facile redox method. The as-synthesized P/CoNiO₂-CNT hybrid catalyst exhibits much higher catalytic activity and long-term stability than P/rGO and P/CNT catalysts for ethanol electrooxidation in alkaline media. Moreover, the obtained P-based hybrid catalysts superior anti-CO poisoning ability.

Materials

All chemical reagents used in this experiment were of analytical grade. Ni(NO₃)₂·6H₂O, Co(NO₃)₂·6H₂O, H₂P Cl₆, NH₄F, NaBH₄, H₂SO₄, HNO₃, ethanol, Nafion, and cerium(III) hexammine bromide (CTAB, Alfa Aesar) were purchased commercially and used as received without further purification. The CNTs with a diameter of 40–60 nm, lengths of 5–15 μm, and a purity of 98% used in this study were purchased from Shenzhen Nanotechnology Port Co., Ltd. (Shenzhen, China).

Preparation of CNTs and CoNiO₂-CNTs

The commercial CNTs were initially treated by a typical hydrothermal method.³⁴ Raw-CNT powders were dispersed in a H₂SO₄-HNO₃ solution (8.0 M for each acid) at a bath temperature of 80 °C and then treated for 2 h under hydrothermal condition. The product was washed with deionized water and dried in a vacuum oven at 70 °C for 12 h for further use.

The CoNiO₂-CNT hybrid composites were obtained through a hydrothermal process and a subsequent high-temperature calcination, in which 50 mg acid-treated CNTs, 0.29 g Ni(NO₃)₂·6H₂O, 0.58 g Co(NO₃)₂·6H₂O, 0.90 g urea, and 0.22 g NH₄F were one-step dissolved in 90 mL deionized water and then ultrasonicated for 60 min. The as-obtained suspension was then transferred into a Teflon-lined stainless-steel autoclave (larger than the total volume of 2/3) and hydrothermally treated at 140 °C for 7 h. After being cooled down to room temperature, the resulting products were filtered and washed with abundant deionized water and ethanol to remove the residues. The cleaned products were placed in a vacuum oven for 12 h at 70 °C. After this, the dried samples were placed in a N₂-protected furnace, and the temperature was slowly increased to 400 °C and maintained for another 2 h. The yielded products were denoted as CoNiO₂/CNT hybrid composites.

Preparation of the Pt/CoNiO₂-CNT catalysts

The P/CoNiO₂-CNT hybrid catalysts were obtained through an impregnation method using NaBH₄ and CTAB as reducing and

protective agents, respectively; herein, the theoretical loading of P on the CoNiO₂-CNT surface was fixed at 20%. Typically, 50 mg of CoNiO₂/CNTs and 3.3 mL of 18.96 mM H₂P Cl₆ were initially added to a 60 mL mixture solution of ethanol/water (1:1, v/v ratio). After vigorous stirring for 0.5 h, 20 mL freshly prepared reducing solution (40 mg NaBH₄ and 15 mg CTAB) was slowly added dropwise to the above mentioned mixture solution under vigorous stirring condition. The resulting solution was continuously stirred for another 24 h and then washed with deionized water. The received solid composites were dried in a vacuum oven at 80 °C for 5 h and denoted as P/CoNiO₂-CNTs (Scheme 1). For better comparison, the P particles on acid-treated CNTs and rGO (20% P) were also prepared using a similar experimental method, in which rGO was synthesized via a modified Hummers method.³⁵

Spectroscopic characterizations

The structures, components, and morphologies of the samples were characterized by scanning electron microscopy (SEM, FEI Quanta 200 FEG, Holland), transmission electron microscopy (TEM, JEM-2100F, Japan), high-resolution transmission electron microscopy (HRTEM), energy-dispersive X-ray spectroscopy (EDS, FEI Quanta 200 FEG, Holland), X-ray diffraction (XRD, Rigaku D/MAX 2500/PC (Japan) diffractometer with Cu Kα radiation), energy-dispersive spectroscopy (EDX, FEI Quanta 200 FEG, Holland), Raman spectroscopy, and X-ray photoelectron spectroscopy (XPS, JPS-9010TR (Japan) with Mg Kα radiation). Inductively coupled plasma analysis (ICP, IRIS Intrepid II XSP) was used to determine the real metal loading of the as-prepared catalysts.

Electrochemical measurements

A general three-electrode system was used to examine all the electrochemical data via a CHI 660C electrochemical working station at room temperature. A glassy carbon electrode, Pt foil, and saturated calomel electrode (SCE) were used as the working, counter, and reference electrodes, respectively. The glassy carbon electrode was first polished by Al₂O₃ powder and then subsequently cleaned in ethanol and water. The working electrodes were prepared as follows: 2.0 mg catalyst was

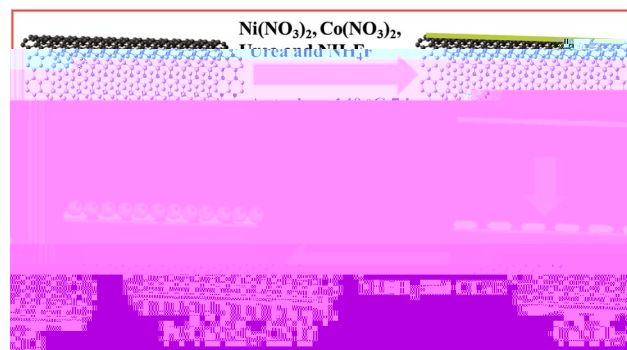


Fig. 1 Schematic of the preparation process of the Pt/CoNiO₂-CNT composite.

dispersed in 400 μL $\text{H}_2\text{O}/\text{C}_2\text{H}_5\text{OH}$ ($v/v = 1:1$) and ultrasonicated for 5 min to form a uniform catalyst ink. Then, 5 μL of catalyst ink was pipetted on the glassy carbon electrode surface ($\phi = 3$ mm); after drying, 5 μL diluted Nafion (0.5%) was dropped on the catalyst to avoid leaching. The Pt loading concentration on the working electrode is ca. $70.8 \mu\text{g cm}^{-2}$.

CO stripping cyclic voltammeter (CV) was used to evaluate the electrochemical active surface area (EAS) of different catalysts in a 1.0 M KOH solution. First, CO was purged in a 1.0 M KOH solution, then a constant potential of -0.3 V (vs. SCE) was set, and the system was continued for 45 min, during which the CO gas was continuously bubbled in the solution. In the initial 30 min, and then, N_2 gas was bubbled in the solution for 15 min to remove the dissolved CO gas. After this, typical CV curves in consecutive cycles were obtained in the solution in the range from -0.8 V to 0.3 V at a scan rate of 50 mV s^{-1} . The ethanol electrochemical oxidation was investigated in a N_2 -saturated 1.0 M KOH + 0.5 M $\text{CH}_3\text{CH}_2\text{OH}$ solution at a scan rate of 50 mV s^{-1} for all the CV cycles. The long-term stability was determined at a potential of 0.3 V for 3600 s. All the electrochemical tests were carried out at ambient temperature (25 \pm 1 $^\circ\text{C}$).

Schematic synthesis of Pt/CoNiO₂-CNTs

The preparation process for the Pt/CoNiO₂-CNT catalyst is shown in Scheme 1. The acid-treated CNTs were initially mixed with $\text{Ni}(\text{NO}_3)_2$, $\text{Co}(\text{NO}_3)_2$, urea, and NH_4F in deionized water via violent ultrasonic treatment for one hour. The resulting solution was transferred in an autoclave and heated to 140 $^\circ\text{C}$ for several hours. After treatment, the Co-Ni hydroxide species were homogeneously distributed on the surface of the acid-treated CNTs. After calcination at 400 $^\circ\text{C}$ for several hours, the porous Co-Ni oxide species were formed on the CNT surface. After this, the added PtCl_6^{2-} ions strongly adsorbed on the surface of Co-Ni oxides/CNTs via electrostatic interaction force. After the mixture solution of NaBH_4 and CTAB was added, the precursor PtCl_6^{2-} ions slowly reduced to Pt seed crystals in the initial stage. Through interaction with the induced CTAB, the Pt crystals formed a special structure in the subsequent growth process. After several hours, the surfactant and various impurities were removed, and the large catalyst was received. The real Pt metal loading on the CoNiO₂-CNT supports was decided by the inductively coupled plasma (ICP) method. The test results show that the percentage of Pt is 21.3% on the Pt/CoNiO₂-CNT hybrid catalyst, which is consistent with the theoretical results.

XRD patterns and Raman spectrum analysis

The as-prepared composites were initially evaluated by X-ray diffraction (XRD). As shown in Fig. 1A, the XRD pattern shows that the main peaks of the prepared samples are consistent with the standard patterns of CoNiO₂ (JCPDS: 10-0188). In addition, some small messy peaks are detected, which can be ascribed to the doped CoOOH species.³⁶ After inducing Pt particles, the

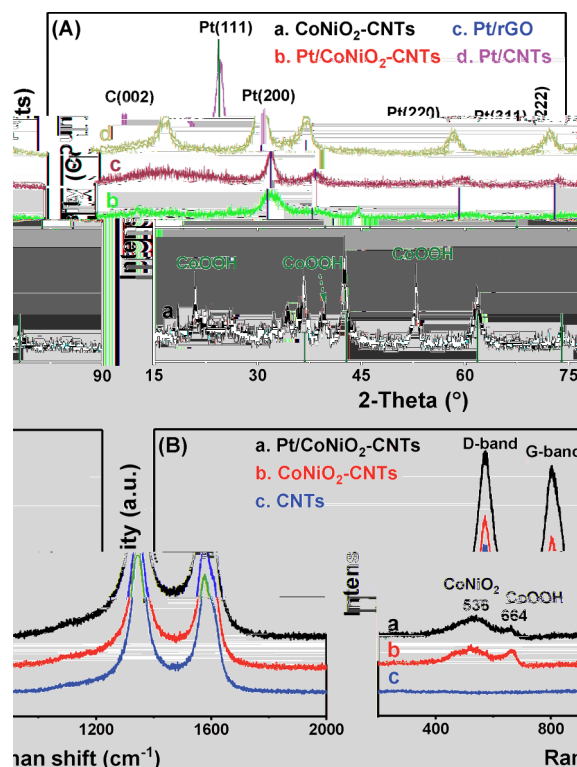


Fig. 1 (A) XRD patterns of (a) CoNiO₂-CNTs, (b) Pt/CoNiO₂-CNTs, (c) Pt/rGO and (d) Pt/CNTs. (B) Raman spectrum of (a) Pt/CoNiO₂-CNTs, (b) CoNiO₂-CNTs, and (c) CNTs.

XRD patterns (Fig. 1A) show that all samples exhibit five main peaks located at 39.8 , 46.2 , 67.5 , 81.3 , and 85.7 $^\circ$, which belong to the face-centered cubic structure of metal Pt (111), (200), (220), (311), and (222), respectively (JCPDS: 04-0802).³⁷ It should be noted that a typical peak located at 26 $^\circ$ is derived from the diffraction pattern of the carbon (002) plane.³⁸ Compared with that of Pt/rGO and Pt/CNTs, the intensity of the peak for Pt/CoNiO₂-CNT hybrid material is weaker, and the widths of the peaks are much broader; this indicates that the particles of Pt on CoNiO₂-CNTs are much smaller than others. In addition, an apparent peak shift could be observed for Pt (220) on Pt/CoNiO₂-CNTs in comparison with the case of other catalysts; this indicates that some Pt atoms might coexist in the synthesized composite. Generally, the Scherrer equation is used to calculate the size of the Pt particles. The average particle size of the Pt particles is estimated by the following equation:³⁹

$$D = K\lambda/\beta \cos \theta \quad (1)$$

where D (nm) is the calculated average diameter of the Pt particles, λ is the selected wavelength of X-ray (0.154056 nm for $\text{Cu K}\alpha$), K is the Scherrer constant (0.89), θ is the Bragg diffraction angle, and β is the half height width of the peak in radians. The average particle size of different catalysts was calculated to be 3.3 , 4.1 , and 5.7 nm for the Pt particles on CoNiO₂-CNT, rGO, and CNT supports, respectively. The smallest particle size indicates that the CoNiO₂-CNT support is beneficial to minimize the particle distribution, which may be due to the much stronger interaction between Pt particles and CoNiO₂.

Raman spectra are further used to characterize the modification process and deconvoluted scattering peaks. As shown in Fig. 1B, all the materials exhibit obvious characteristic peaks located at 1348 and 1583 cm^{-1} , which correspond to the D-band and G-band, respectively. Generally, the D-band is contributed from the vibrations of sp^3 carbon atoms in the disordered structures, and the G-band originates from the domains of graphitic sp^2 carbon atom vibrations in the composite structures.³⁵ Specifically, P/CoNiO₂-CNTs and CoNiO₂-CNTs show additional peaks at 536 and 664 cm^{-1} , which are considered to have originated from the scattering peaks of CoNiO₂ and CoOOH, respectively.^{40,41} The results further demonstrate that CoNiO₂ is clearly modified on acid-treated CNTs.

Morphology characterization and XPS analysis

The morphologies, elements, and particle size distributions of P/CoNiO₂-CNTs are characterized by TEM images and EDS mapping. As shown in Fig. 2a, the TEM images of P/CoNiO₂-CNTs show that the particles of P are well-dispersed on the CoNiO₂ modified acid-treated CNT surface. The particle size distribution of P (see Fig. 2b and S1†) obtained from randomly selected 100 particles shows that the average particle size is 3.1 nm, which is consistent with the calculated XRD results. The high-resolution TEM image (see Fig. 2c) exhibits three different types of fringe spacings at approximately 0.34, 0.241, and 0.224 nm corresponding to CNTs (002), CoNiO₂ (111), and P (111) in the planar directions, respectively. The EDS spectra of P/CoNiO₂-CNTs (see Fig. S2†) show that the elements C, O, Co, Ni, and P are clearly exhibited in the large composition. Additionally, as shown in Fig. 2d–g, the elements P, Co, Ni, and O are consistently distributed throughout the composite; this further indicates that the P particles are well-dispersed on the treated CoNiO₂-CNT hybrid material.

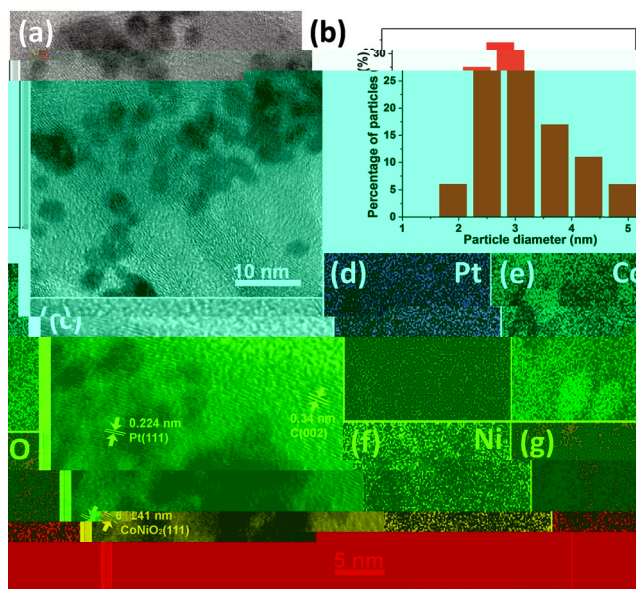


Fig. 2 (a) TEM image and (b) particle size distribution of Pt/CoNiO₂-CNTs; (c) High-resolution TEM image of Pt/CoNiO₂-CNTs; EDS mapping of (d) Pt, (e) Co, (f) Ni, and (g) O for Pt/CoNiO₂-CNTs.

The XPS technique provides information on the composition of the catalyst and the corresponding chemical valence states of the designed composites. The entire XPS spectrum is initially corrected by the high-resolution C 1s spectrum. As shown in Fig. 3a, the C 1s spectrum is mainly deconvoluted into three peaks: 284.0 eV (sp^2 C=C), 284.8 eV (sp^3 C-C), and 286.0 eV (C-O). The full-range XPS spectrum of the as-prepared P/CoNiO₂-CNTs (see Fig. S3†) shows that the material is composed of C, O, P, Ni, and Co. As shown in Fig. 3b, the high-resolution P 4f peaks can be deconvoluted into three pairs of peaks for P 4f_{7/2} (70.8, 71.4, and 72.8 eV) and P 4f_{5/2} (74.1, 74.8, and 76.1 eV), in which the binding energies at 70.8 and 74.1 eV are related to metallic P⁰, the binding energies at 71.4 and 74.8 eV are ascribed to P²⁺ from PO or P(OH)₂, and the binding energies located at 72.8 and 76.1 eV are attributed to P₂O₃.^{38,42} As shown in Fig. 3c, the high-resolution Co 2p with Co 2p_{3/2} and Co 2p_{1/2} peaks in the P/CoNiO₂-CNT composite is observed, in which the binding energies for metallic Co⁰ are located at 778.0 and 797.7 eV, indicating that partial P-Co alloys are formed.⁴³ The binding energies of the Co²⁺ species are located at 783.4 and 801.0 eV, and those of the Co³⁺ species are located at 781.4 and 799.3 eV, respectively.⁴³ It should be noted that there are two other pairs of peaks at higher binding energies, which can be considered as satellite peaks from cobalt (hydro)oxide. The high-resolution Ni 2p of P/CoNiO₂-CNTs is shown in Fig. 3d, in which the two relative high spike peaks at 856.6 and 874.2 eV are ascribed to the Ni²⁺ oxidation state of Ni 2p_{3/2} and Ni 2p_{1/2}, respectively.³⁴ The other two peaks observed at 859.1 and 877.1 eV are ascribed to Ni 2p_{3/2} and Ni 2p_{1/2} of Ni³⁺, respectively.⁴⁴ It is noteworthy that a pair of peaks at high binding energies can be clearly observed, which is derived from the shake-up satellite peaks of nickel (hydro)oxide.

Electrochemical performance analysis

CO-stripping voltammetry is an effective method to evaluate the removal ability of intermediates (especially CO_{ads}), but can also

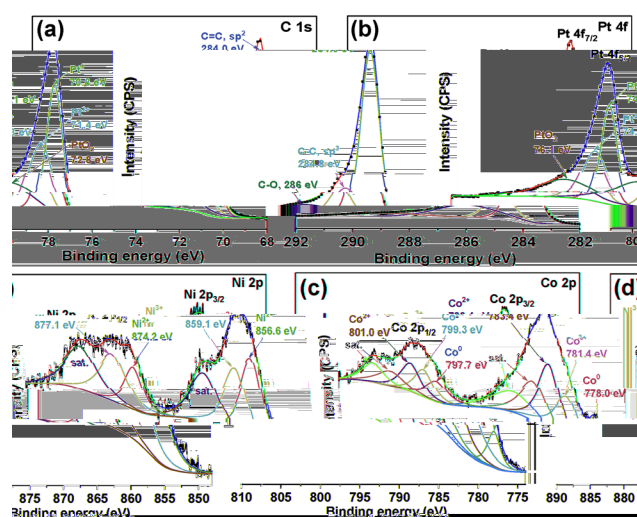


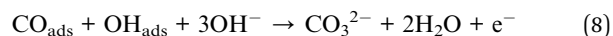
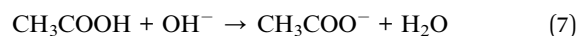
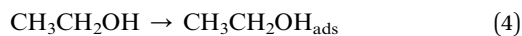
Fig. 3 High-resolution XPS spectrum of (a) C 1s, (b) Pt 4f, (c) Co 2p, and (d) Ni 2p for Pt/CoNiO₂-CNTs.

res l s sho ha he ca al ic performance and an i-poisoning abili of o r de eloped h brid ca al s are be er han hose of mos of e er repor ed P -based ca al s s for e hanol elec ro- o ida ion in an alkaline sol ion. More impor anl , as sho n in Fig. 5B, he Tafel slope of P /CoNiO₂-CNTs is 205 mV dec⁻¹ (similar o ha of he commercial P /C), hich is lo er han ha of P /rGO (422 mV dec⁻¹) and P /CNTs (218 mV dec⁻¹), sho ing m ch fas er reac ion kine ics.⁴⁷

Apar from he elec roca al ic ac i i , long- erm s abili is ano her signifikan cri erion o e al a e he . sef lness of a ca al s . As sho n in Fig. 6, ime-dependen c rren densi es are in es iga ed in a sol ion of 1.0 M KOH + 0.5 M e hanol for 3600 s a a fi ed po en ial of -0.3 V. I can be seen ha all ca al s s ha e rela i el high ini ial c rren densi es, hich hen s ffer a rapid recession s age n il he reach rela i el s ead s a es. The higher ini ial c rren densi es res l from higher e hanol concen ra ions, and he sharp deca id e o he decrease in he e hanol concen ra ion gradien and he poisoning of he acc m la ed in ermedia e species. I is or h no ing ha he c rren densi of P /CoNiO₂-CNTs is signifikan higher han ha of he P /rGO and P /CNT ca al s s in he hole process, and he final c rren densi of P /CoNiO₂-CNTs (37.7 mg cm⁻¹ P) is 55.4- and 2.2-fold higher han ha of P /rGO and P /CNTs, respec i el .

Mechanism discussion

The e cellen elec rochemical ac i i and long- erm s abili of P /CoNiO₂-CNTs for e hanol elec ro- o ida ion co ld be ascribed o he s nergis ic effec of he ell-dispersed small P par icles and he CoNiO₂-modified CNT s bs ra e. As sho n in Scheme 2, he specific s nergis ic ca al ic process can be . nders ood, and he differen s eps can be ded ced as follo s:^{5,48}



As is ell kno n, he s rface of CoNiO₂ carries a nega i e charge nder alkaline condi ions beca se he h dro l gro p (-OH) adsorbs on o he s rface of CoNiO₂; his res l s in he forma ion of CoNiO₂-OH_{ads} species on he h brid s ppor . Herein, . pon con in o sl increasing he po en ials on he anode, he ac i e si es of P on he h brid ca al s ill adsorb he e hanol molec les from he sol ion, and P -CH₃CH₂OH_{ads} species ill be formed. Then, he P -CH₃CH₂OH_{ads} species ill be o idi ed o P

o the synthesized P/CoNiO₂-CNT catalysts, and the final products have been analyzed by C2 and C1 pathways. The superior electrocatalytic performance of the designed catalysts reported herein highlights an effective methodology to achieve ultrahigh catalytic activity for ethanol in alkaline media, indicating potential application prospects of this catalyst in direct alkaline ethanol fuel cells.

ft

There are no conflicts to declare.

This work was supported by the National Natural Science Foundation of China (21363003, 21165004, 21163002), National Science Foundation of Guangxi Province (2014GXNSFGA118008, 2014GXNSFFA118003), BAGUI scholar program (2014A001), and Project of Talents Highland of Guangxi Province.

- 1 X. H. ang, Z. Zhao, L. Cao, Y. Chen, E. Zh , Z. Lin, M. Li, A. Yan, A. Ze l, Y. M. Wang, X. D an, T. M eller and Y. H ang, *Science*, 2015, **348**, 1230–1234.
- 2 D. Wang, H. L. Xin, R. Ho den, H. Wang, Y. Y , D. A. M ller, F. J. DiSal o and H. D. Abr ña, *Nat. Mater.*, 2013, **12**, 81–87.
- 3 S. K. Na araj, C.-H. Wang, H.-C. H ang, H.-Y. D , L.-C. Chen and K.-H. Chen, *ACS Sustainable Chem. Eng.*, 2015, **3**, 302–308.
- 4 B. P. Se ler, Z. Zh ang, J. A. Wi kopf and Y. Yan, *Nat. Nanotechnol.*, 2016, **11**, 1020–1025.
- 5 B. M. Daas and S. Ghosh, *J. Electroanal. Chem.*, 2016, **783**, 308–315.
- 6 Z. Li and Q. Ni , *ACS Sustainable Chem. Eng.*, 2014, **2**, 533–536.
- 7 L. Li, J. Zhang, Y. Li , W. Zhang, H. Yang, J. Chen and Q. X , *ACS Sustainable Chem. Eng.*, 2013, **1**, 527–533.
- 8 X. Yang, X. Li , X. Meng, X. Wang, G. Li, C. Sh , L. Jiang and C. Wang, *J. Power Sources*, 2013, **240**, 536–543.
- 9 Y. Shen, K. Xiao, J. Xi and X. Qi , *J. Power Sources*, 2015, **278**, 235–244.
- 10 L. Zhang and Y. Shen, *ChemElectroChem*, 2015, **2**, 887–895.
- 11 Y. Shen, M. Z. Zhang, K. Xiao and J. Xi, *ChemCatChem*, 2014, **6**, 3254–3261.
- 12 Y. Shen, Z. Zhang, K. Xiao and J. Xi, *Phys. Chem. Chem. Phys.*, 2014, **16**, 21609–21614.
- 13 Q. He, Y. Shen, K. Xiao, J. Xi and X. Qi , *Int. J. Hydrogen Energy*, 2016, **41**, 20709–20719.
- 14 Q. Li , J. Fan, Y. Min, T. W , Y. Lin and Q. X , *J. Mater. Chem. A*, 2016, **4**, 4929–4933.
- 15 Q. Li , Y. Lin, J. Fan, D. L , Y. Min, T. W and Q. X , *Electrochem. Commun.*, 2016, **73**, 75–79.
- 16 Q. Li , K. Jiang, J. Fan, Y. Lin, Y. Min, Q. X and W.-B. Cai, *Electrochim. Acta*, 2016, **203**, 91–98.

- 17 M. Li, Z. Zhao, T. Cheng, A. For nelli, C.-Y. Chen, R. Y , Q. Zhang, L. G , B. V. Merino , Z. Lin, E. Zh , T. Y , Q. Jia, J. G o, L. Zhang, W. A. Goddard, Y. H ang and X. D an, *Science*, 2016, **354**, 1414–1419.
- 18 L. B , N. Zhang, S. G o, X. Zhang, J. Li, J. Yao, T. W , G. L , J.-Y. Ma, D. S and X. H ang, *Science*, 2016, **354**, 1410–1414.
- 19 Q. Wang, Z. Tang, L. Wang, H. Yang, W. Yan and S. Chen, *ChemistrySelect*, 2016, **1**, 6044–6052.
- 20 J. Zhang, X. Yang, H. Shao, C.-C. Tseng, S. Tian, W. H , C. Jing, J. Tian and Y. Zhao, *Fuel Cells*, 2017, **17**, 115–122.
- 21 X. Yang, M. Zhen, G. Li, X. Li , X. Wang, C. Sh , L. Jiang and C. Wang, *J. Mater. Chem. A*, 2013, **1**, 8105–8110.
- 22 Y. Zhao, X. Yang, J. Tian, F. Wang and L. Zhan, *Mater. Sci. Eng., B*, 2010, **171**, 109–115.
- 23 Y. Shen, B. Gong, K. Xiao and L. Wang, *ACS Appl. Mater. Interfaces*, 2017, **9**, 3535–3543.
- 24 J. S. Spendelo and A. Wiecko ski, *Phys. Chem. Chem. Phys.*, 2007, **9**, 2654–2675.
- 25 S. Sharma and B. G. Polle , *J. Power Sources*, 2012, **208**, 96–119.
- 26 P. K. Shen and C. X , *Electrochem. Commun.*, 2006, **8**, 184–188.
- 27 C. X , Z. Tian, P. Shen and S. P. Jiang, *Electrochim. Acta*, 2008, **53**, 2610–2618.
- 28 C. Y an, J. Li, L. Ho , X. Zhang, L. Shen and X. W. Lo , *Adv. Funct. Mater.*, 2012, **22**, 4592–4597.
- 29 Y. Yang, L. Ren, C. Zhang, S. H ang and T. Li , *ACS Appl. Mater. Interfaces*, 2011, **3**, 2779–2785.
- 30 J. Li , Y. Li, X. H ang, G. Li and Z. Li, *Adv. Funct. Mater.*, 2008, **18**, 1448–1458.
- 31 P. Li and H. C. Zeng, *Adv. Funct. Mater.*, 2017, **27**, 1606325.
- 32 X.-F. L , L.-F. G , J.-W. Wang, J.-X. W , P.-Q. Liao and G.-R. Li, *Adv. Mater.*, 2016, **29**, 1604437.
- 33 H. Cheng, Y. S , P.-Y. K ang, G.-F. Chen and Z.-Q. Li , *J. Mater. Chem. A*, 2015, **3**, 19314–19321.
- 34 Y. Zhao, X. Yang, J. Tian, F. Wang and L. Zhan, *Int. J. Hydrogen Energy*, 2010, **35**, 3249–3257.
- 35 X. Peng, D. Chen, X. Yang, D. Wang, M. Li, C.-C. Tseng, R. Panneersel am, X. Wang, W. H , J. Tian and Y. Zhao, *ACS Appl. Mater. Interfaces*, 2016, **8**, 33673–33680.
- 36 J. H ang, J. Chen, T. Yao, J. He, S. Jiang, Z. S n, Q. Li , W. Cheng, F. H , Y. Jiang, Z. Pan and S. Wei, *Angew. Chem., Int. Ed.*, 2015, **127**, 8846–8851.
- 37 Y. Zhao, X. Yang, J. Tian, F. Wang and L. Zhan, *J. Power Sources*, 2010, **195**, 4634–4640.
- 38 X. Yang, J. Zheng, M. Zhen, X. Meng, F. Jiang, T. Wang, C. Sh , L. Jiang and C. Wang, *Appl. Catal., B*, 2012, **121–122**, 57–64.
- 39 D. Chen, Y. Zhao, Y. Fan, X. Peng, X. Wang and J. Tian, *J. Mater. Chem. A*, 2013, **1**, 13227–13232.
- 40 X. Leng, Y. Shao, L. W , S. Wei, Z. Jiang, G. Wang, Q. Jiang and J. Lian, *J. Mater. Chem. A*, 2016, **4**, 10304–10313.
- 41 T. Pa por e, L. Mendo a, M. Cassir, M. C. Bernard and J. Chi o , *J. Electrochem. Soc.*, 2005, **152**, C49–C53.
- 42 L. Wang, Z. Tang, W. Yan, Q. Wang, H. Yang and S. Chen, *J. Power Sources*, 2017, **343**, 458–466.

43 X. Yang, H. Li, A.-Y. Li, S. Min, Z. Idriss, M. N. Hedhili, K.-W. Hong, H. Idriss and L.-J. Li, *Nano Energy*, 2016, **25**, 42–50.

44 Y. Feng, X. Yang and U. Paik, *Chem. Commun.*, 2015, **52**, 1633–1636.

45 T. Vidaković, M. Christoff and K. S. Ndmacher, *Electrochim. Acta*, 2007, **52**, 5606–5613.

46 L. Ma, D. Chen and R. Chen, *Int. J. Hydrogen Energy*, 2012, **37**, 11185–11194.

47 C. Xiao, S. Li, J. Zhang and D. MacFarlane, *J. Mater. Chem. A*, 2017, **5**, 7825–7832.

48 K. Arshko, B. Haleji, M. Padilla, P. Anasso and E. A. Bao, *Int. J. Hydrogen Energy*, 2017, **42**, 12585.

Kleijni,